Communication

Novel Janus Fibrous Membranes with Enhanced Directional Water Vapor Transmission

Shengnan Tang, Haohong Pi, Yingying Zhang, Jing Wu * and Xiuqin Zhang *

Beijing Key Laboratory of Clothing Materials R&D and Assessment, Beijing Engineering Research Center of Textile Nanofiber, School of Materials Science and Engineering, Beijing Institute of Fashion Technology, Beijing 100029, China
* Correspondence: a.wujing@163.com (J.W.); clyzxq@bift.edu.cn (X.Z.)

check for updates

Abstract: Novel hydrophobic/hydrophilic Janus fibrous membranes, the poly[4,4'-methylenebis (phenylisocyanate)-alt-1,4-butanediol/di(propylene glycol)/plycaprolactone] (PU) fibrous membrane as the hydrophobic layer and cellulose acetate (CA) fibrous membrane as the hydrophilic layer, were fabricated by the so-called "layer-by-layer" electrospinning technology. A series of the PU/CA Janus membranes with different electrospinning time of the CA layers by which the thickness of hydrophilic layer can be controlled were also prepared to uncover its influence on the directional water vapor transmission. The results showed that water vapor transmission capability from the hydrophobic side to the hydrophilic side of the PU/CA Janus fibrous membrane was enhanced rather than that from the reverse direction of the same membrane. The optimal water vapor transmission capacity existed when the electrospinning time of CA fibrous membrane reached 15 min. Such enhanced water vapor transmission originated because of the asymmetric wettability of the Janus membrane and the strong force to draw tiny water droplet from the hydrophobic side to the hydrophilic side. The novel understanding is useful for facile designing and fabrication of efficient moisture permeable fabrics and clothing.

Keywords: Janus fibrous membrane; hydrophobic; hydrophilic; electrospinning; directional water vapor transmission

1. Introduction

Directional water vapor or moisture transport has received extensive attentions and has driven scientists to develope materials with multi-functions and techniques for many kinds of applications, such as fog harvesting, functional fabrics or textiles, and so on [1–7]. Efficient water vapor transmission has been considered as an ideal way to provide a proper microclimate to satisfy the personal comfort. Learning from the nature, researchers found that the Namib Desert beetles and Texas horned lizard drive the one-way transmission of water droplets in foggy conditions on their typical bumpy backs with alternating hydrophilic and hydrophobic regions; the honeycomb surface of the scales increases the surface roughness and support more condensation foci to survive [8–11]. By exploring the creatures with excellent directional water transport ability, tremendous methods in attempting to prepare artificial materials with excellent directional water transport or capture capability have been proposed [12–17].

Previous studies revealed that fibrous membrane with wettability gradient or contrast in the thickness direction exhibit unique directional water transport phenomena. Wang et al. reported that hydrophobic-to-hydrophilic gradient across the thickness of a fabric can guide directional water-transport from the hydrophobic side to the hydrophilic side, but no water transport takes place in the opposite direction unless an extra force is applied [18,19]. Such unidirectional water penetration phenomenon was also reported by our group [20] and referred to as "water diode" [21,22] or "directional wicking" [1,23].

The unique directional water transport can alternatively be achieved by abruptly changing the wettability from hydrophobicity to hydrophilicity along the thickness of the fibrous membrane, such as Janus membrane which is a "double-side" membrane with asymmetric properties on either side of the membrane or at membrane surfaces. These properties are primarily derived from different components and/or structures, and are expressed in the form of hydrophilic/hydrophobic or positive/negative surface charges [24–29].

Despite the reports about directional water transport materials, the study on enhancing water vapor transmission capability of fabrics or clothing membranes by directional driven property of water Janus membrane is scarce. Herein, hydrophobic poly [4,4'-methylenebis (phenylisocyanate)-alt-1,4-butanediol/di(propylene glycol)/plycaprolactone] (PU) and hydrophilic cellulose acetate (CA) that exhibit great possibility for application in efficient moisture permeable fabric design and fabrication were chosen as the raw materials. The hydrophobic–hydrophilic PU/CA Janus fibrous membrane was fabricated by the "layer-by-layer" electrospinning technique which shows facile and excellent maneuverability in constructing asymmetric wettability in the thickness direction of nanofibrous membrane. The water vapor transmission capacities from the hydrophobic side to the hydrophilic side and the reverse direction of the Janus membranes were measured. Furthermore, the electrospinning time of hydrophilic side by which the thickness can be controlled were taken into consideration to uncover the optimal water vapor transmission capacity.

2. Materials and Methods

2.1. Materials

Poly [4,4'-methylenebis (phenylisocyanate)-alt-1,4-butanediol/di(propylene glycol)/plycaprolactone] (PU, Mn = 170,000) and cellulose acetate (CA, Mn = 50,000) were obtained from Sigma-Aldrich (St. Louis, MO, USA). *N,N*-dimethylformamide (DMF), tetrahydrofuran (THF), dichloromethane (DCM), ethanol, and acetone were bought from Beijing Yili Fine Chemical Co. (Beijing, China). Skim cotton fabric (21 ^{S} × 21 ^{S}, 110 cm × 100 cm, 80 cm × 15 cm) was supplied by Beijing Aoruikang Technology Development Co., Ltd. All the chemicals were of analytical grade and used as received without any pretreatment.

2.2. Preparation of the Moisture-Penetrability Janus Membranes

The precursor solution was prepared by dissolving the sufficiently dried CA powder in DMF and acetone solvent (the mass ratio was 2:1) at a series of concentration (7.5 wt %, 10 wt %, 12.5 wt %) and stirred for 8 h at room temperature. An electrospinning machine was employed to fabricate the membranes. Nearly 4 mL precursor solution was placed in a 5-mL syringe, and the flow velocity was controlled to 1.0 mL/h by the injection pump. The syringes were periodically scanned in the horizontal direction with a width of 90 cm. In order to form cellulose acetate fibers with different diameters, different metal needle nozzles with the inner diameters of 0.6, 0.8, 1.0, and 1.2 mm (named as 6G, 8G, 10G and 12G) were equipped. A skim cotton fabric was covered on the drum (200 r/min) as the collector. The distance between the needle tip and the collector was 15 cm, and the voltage was set as 8~15 kV, respectively. The electrospinning process was adjusted for 5, 10, 15, 20, 25, and 30 min to obtain the CA electrospun fibrous layers with different thicknesses, and then the as-prepared CA membranes were directly used as the substrate for the next step without any treatment.

The PU pellets were dissolved in DMF and THF solvent (the mass ratio was 9:1) at 40 °C for 8 h to obtain a uniform solution with different concentrations (10, 12.5, 15, 17.5, and 20 wt %). Then, the as-prepared precursor solutions were loaded onto the same electrospinning machine, and the feed rate of the solutions was 0.8 mL/h. The above as-prepared CA fibrous layers were used as the collector. The PU electrospun fibrous layers were then fabricated by the similar method as the CA layer. After 15 min, the PU/CA Janus fibrous membranes were successfully fabricated.

2.3. Instruments and Characterization

The microstructures of the membranes were characterized using scanning electron microscopy (JSM-6700F, Tokyo, Japan). The diameters of the PU and CA nanofibers were measured according to the SEM images. The water contact angles were tested on an OCA 20 contact-angle system (Dataphysics, Stuttgart, Germany) at room temperature. Deionized water droplets (3 μL) were dropped onto the fibrous membrane surface. Each contact angle value was obtained by measuring at six different positions of the same sample to get the average value. The water adhesion forces were measured using the high-sensitivity micro-electro-mechanical balance system (Data-Physics DCAT11, Stuttgart, Germany). To measure the relationship between water adhesion force and the distance of fiber membranes, the water droplet (5 μL) was suspended with a metal cap and controlled to contact with the surface of the membrane with a constant speed of 0.005 mm·s^{-1}, and then controlled to leave. The force–distance curve was recorded at the real-time. To measure the relationship between water adhesion force and time, the water droplet was controlled to contact the membrane surface and keep contacting until it was adsorbed. The force–time curve was recorded. The chemical compositions of fibrous membranes were characterized by Fourier transform infrared spectrometry (FTIR) on Nicolet 8700 FT-IR spectrometry (Madison, WI, USA) in the wave range from 400 to 4000 cm^{-1}. Directional water-transport performance was quantitatively measured by the moisture-management tester (MMT) (SDL ATLAS, Ltd., Beijing, China). The specimen was cut into the size of 8 cm × 8 cm and held with sample stages. During the measurement, the membranes were put between two horizontal (top and bottom side) electrical sensors, and saline water (0.21 g ± 0.01 g, 0.9% NaCl, based on AATCC TM 195) was dropped onto the top surface of the membranes in 20 s. Thus, the saline water content on the top and bottom surface of the membranes can be calculated based on the corresponding resistance (in the first 120 s since starting dropping the saline water). All samples were put into the conditioned room (21 ± 1 °C, relative humidity 65 ± 2%, refer to ASTM D1776) for at least 24 h prior to testing, horizontally.

3. Results and Discussion

3.1. Fabrication and Morphology of Polyurethane (PU)/Cellulose Acetate (CA) Janus Fibrous Membrane

In this work, poly[4,4′-methylenebis (phenylisocyanate)-alt-1,4-butanediol/di(propylene glycol)/plycaprolactone] (PU) and cellulose acetate (CA) were used as the raw polymers to fabricate the hydrophobic/hydrophilic Janus fibrous membrane. The Janus membrane was fabricated by so-called "layer-by-layer" electrospinning. Accordingly, Figure 1 provides a schematic diagram of the preparation process. PU was dissolved in a solvent mixture of *N*,*N*-dimethylformamide (DMF)/tetrahydrofuran (THF) and was electrospun and collected on an aluminum (Al) foil covered on a rotating drum. The obtained PU fibrous membrane is hydrophobic. After that, the second CA fibrous layer showing hydrophilic properties was fabricated by dissolving CA in the mixture of acetone/dichloromethane (AC/DCM). The hydrophilic CA fibrous layer was deposited on the top of the PU fibrous layer in sequence by seamless coupling with the PU fibrous layer. Finally, when peeled off from the Al substrate, the hydrophobic/hydrophilic Janus fibrous membrane was successfully fabricated.

Electrospinning is widely recognized as a simple top-down method of fabricating materials with different morphologies such as "spheres," "knot-in-fiber structure," and fibers with diameters from tens of nanometers to submicrometers by stretching a viscous conductive fluid into a thin jet via electrostatic force [30]. Among them, the electrospun solutions and electrospun needle nozzles are regarded as the main factors affecting the morphology of the electrospun materials. Therefore, we explored the effects of different concentrations of electrospun solutions and inner diameters of the electrospun needle nozzles on the morphology of nanofibrous materials [31]. Figure 2a–f presents the scanning electron microscope (SEM) images of PU layers which were electrospun with the PU/(DMF/THF 9:1) concentrations of 5 wt %, 7.5 wt %, 10 wt %, 12.5 wt %, 15 wt %, and 17.5 wt %, respectively, and the electropsun needle type 8G (inner diameter~0.8 mm). It is obvious that there are PU spheres at the low concentration of 5 wt %. With the increase of the solution concentration, the amount of PU spheres

decreased. Meanwhile, the PU fibrous structures formed. When the concentration reached to 10 wt %, PU fibrous membrane on which some fibers adhere to each other (pink dotted-circle, in Figure 2c) are obtained. By continuously increasing the concentrations of the electrospun solutions, PU fibrous membrane with uniform fiber distribution are obtained (Figure 2d–f). To prepare the Janus fibrous membrane, the second CA fibrous layer was fabricated with CA/(Ac/DMF) solution and deposited on the top of the PU layer. Figure 2g–i shows the morphologies of CA with the concentrations of 7.5 wt %, 10 wt %, and 12.5 wt %, respectively. It can be seen that at the concentration of 12.5 wt %, CA fibrous membrane can be obtained.
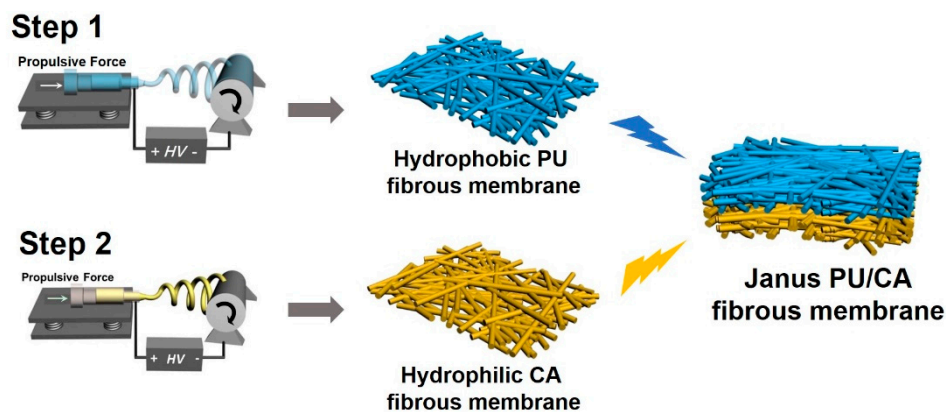

Figure 1. Schematic diagram of the fabrication process of poly[4,4′-methylenebis (phenylisocyanate)-alt-1,4-butanediol/di(propylene glycol)/plycaprolactone] (PU)/cellulose acetate (CA) Janus fibrous membrane. The PU fibrous membrane which is hydrophobic was obtained as the first layer by electrospinning. Then another layer, CA fibrous membrane which exhibits hydrophilic properties, was electrospun onto it and by seamless coupling with the upper PU fibrous layer. When the composited two layers were peeled off from the Al foil substrate, the Janus membrane with wettability contrast was formed.
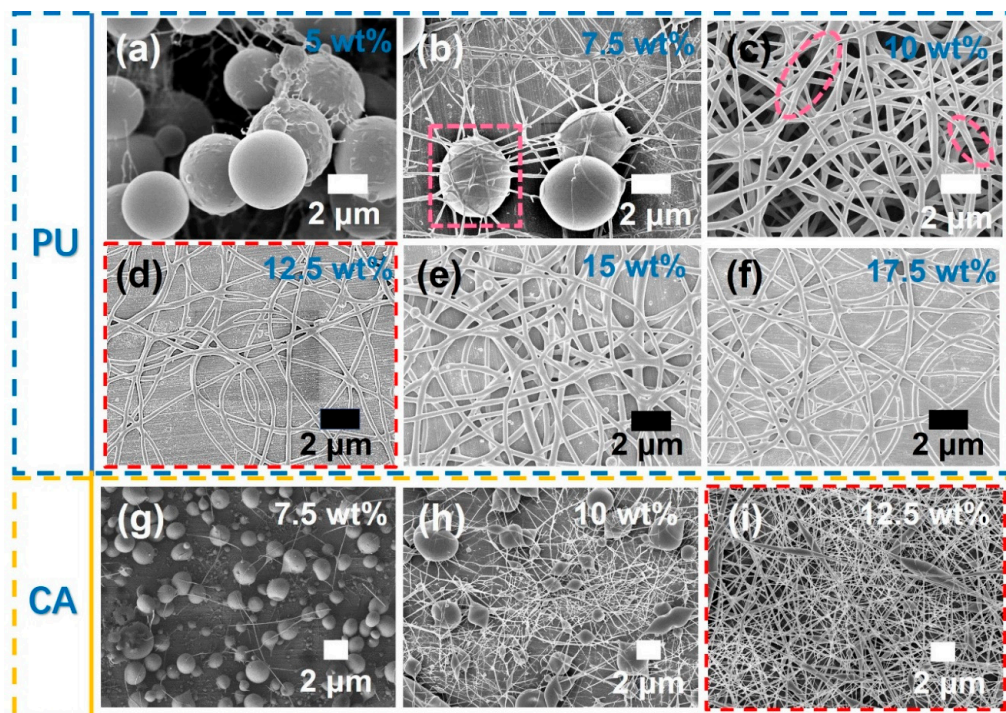

Figure 2. Scanning electron microscope (SEM) images of PU and CA fibrous membrane. PU/(DMF:THF = 9:1) = (**a**) 5 wt %; (**b**) 7.5 wt %; (**c**) 10 wt %; (**d**) 12.5 wt %; (**e**) 15 wt %; (**f**) 17.5 wt %. CA/(Ac:DMF) = (**g**) 7.5 wt %; (**h**) 10 wt %; (**i**) 12.5 wt %.

To explore the influence of the inner diameters of the electrospun needle nozzle on the fibrous morphologies, electrospun needle nozzle with the inner diameters of 0.6 (6G), 0.8 (8G), 1.0 (10G), and 1.2 mm (12G) were equipped during the fabrication process. Figure 3a–d presents the typical SEM images of electrospun PU fibrous membranes with different fiber diameters, which are named as PU-6G, PU-8G, PU-10G, and PU-12G, respectively. The corresponding statistic average diameters (AD) are 380 nm, 669 nm, 1090 nm, and 1110 nm, respectively. Meanwhile, the statistic average fiber diameter of electrospun CA fibrous membranes named CA-6G, CA-8G, CA-10G, and CA-12G are 225 nm, 228 nm, 340 nm, and 354 nm, respectively. Both the PU and CA fiber diameters increased with the increase in inner diameters of the electrospun needle nozzles. Herein, the concentrations of PU and CA were chosen at 12.5 wt %, and the electrospun needle nozzle type was 8G, respectively, under which uniform fibers can be fabricated. When peeled off from the Al foil substrate, a free standing hydrophobic/hydrophilic PU/CA Janus membrane was successfully obtained.
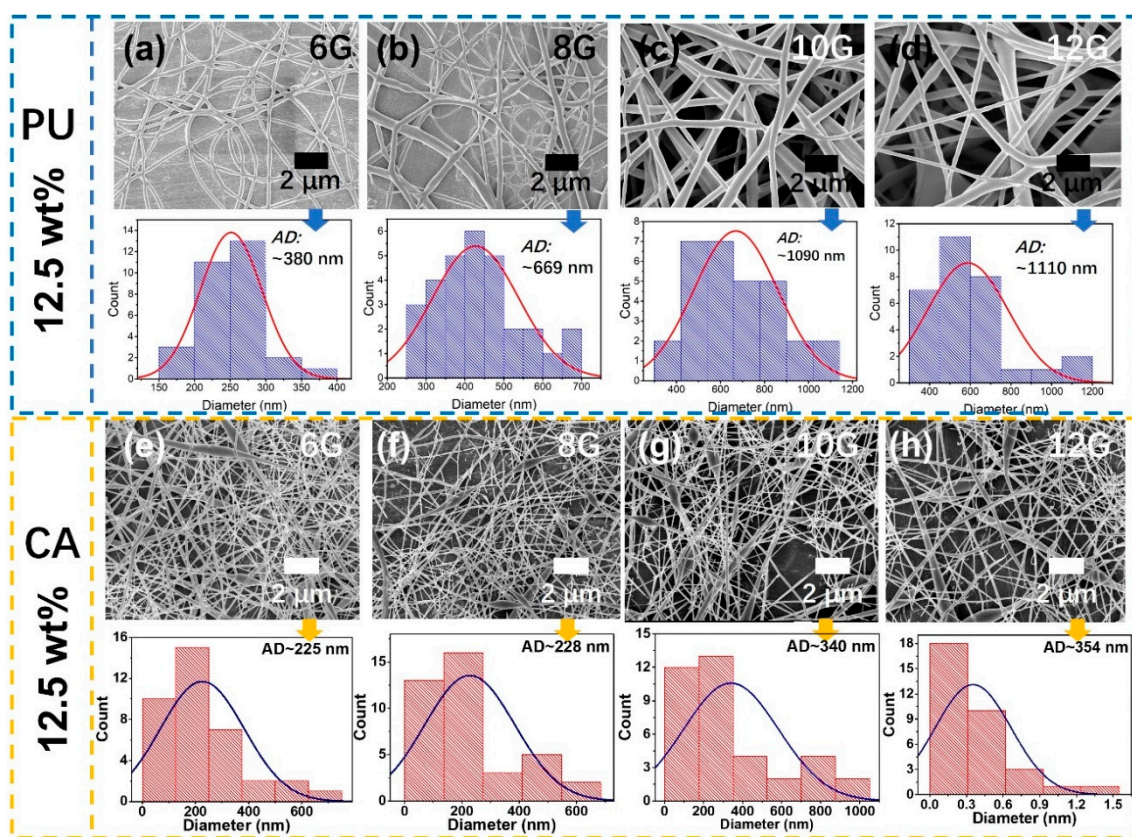

Figure 3. SEM images and statistic average diameters of PU and CA fibrous membrane. The concentrations of both PU and CA electrospun solution are 12.5 wt %, respectively. (**a–d**) SEM images of PU-6G, PU-8G, PU-10G, and PU-12G electrospun fibrous membranes. The statistic average fiber diameters (AD) are 380 nm, 669 nm, 1090 nm, and 1110 nm, respectively (Bar: 2 μm). (**e–h**) SEM images of CA-6G, CA-8G, CA-10G, and CA-12G electrospun fibrous membranes. The AD are 225 nm, 228 nm, 340 nm, and 354 nm, respectively.

3.2. Chemical Characterization and Wettability of As-Prepared Membranes

The Fourier transform infrared spectroscopy (FTIR) was used to characterize the chemical compositions of the PU/ CA Janus electrospun nanofibrous membrane, as well as the solvents (DMF, THF, acetone) that dissolve the electrospun polymers. FTIR was carried out in the range of 400 cm^{-1}–4000 cm^{-1} to analyze and confirm the presence of functional groups [32]. The absorption band of DMF at 1687 cm^{-1} corresponded to the stretching vibration of the C=O vibration [33]. The peak at 1071 cm^{-1} can be assigned to the THF alicyclic ether (C–O–C) stretching vibration [34]. The band

around 1715 cm^{-1} was the characteristic peak of acetone, which can be attributed to the stretching vibration peak of the C=O group [35]. The peaks at 1050 cm^{-1}, 1232 cm^{-1}, 1369 cm^{-1}, and 1743 cm^{-1} of the CA membrane spectra can be assigned to the stretching vibrational peak of the C–O skeleton in ether group, stretching vibration of C–O–C bond, stretching vibration peak of C–CH$_3$, and the stretching vibration of the C=O group, respectively [36–38]. Moreover, there were no characteristic peaks at 1687 cm^{-1} and 1715 cm^{-1}, indicating that there was no DMF and acetone solvent residues in the as-prepared CA electrospun nanofibrous membrane. By analyzing the FTIR characterization of electrospun PU fibrous membrane, it was found that a strong peak appeared at 3328 cm^{-1}, representing the N–H stretching vibration. The peak at 2929 cm^{-1} was the asymmetric vibrations of the –CH$_2$ groups. Since the C=O stretching vibration of the urethane bonds, a medium strong characteristic peak appeared at 1726 cm^{-1}. The absorption band around 1529 cm^{-1} was ascribed to the deformation vibration of N–H bonds in the urethane groups from amide II. The peaks at 1221 cm^{-1} was corresponded to the stretching vibration of the C–N bonds. The bands at 1163 cm^{-1} and 1068 cm^{-1} represented the stretching vibration of the C–O–C groups [38,39]. In addition, there were no characteristic peaks at 1687 cm^{-1} and 1071 cm^{-1} which demonstrated that there were no residues of DMF and THF in the PU electrospun nanofibrous membrane.

Comparing the FTIR spectrum of both sides of the Janus membrane and the pure PU, CA fibrous membranes, it was found that the spectrum of the PU side of the Janus membrane and the PU fibrous membrane were basically consistent, and the CA characteristic peak was not shown in the PU side of the Janus membrane spectrum. However, the spectrum of the CA side of the Janus membrane not only shows the spectrum of CA fibrous membrane, but also shows the characteristic peak of PU fibrous membrane (at 3328 cm^{-1}, 2929 cm^{-1}, 1529 cm^{-1}, and 1163 cm^{-1} in Figure 4a). This phenomenon may be caused by the thicker PU layer and the thinner CA layer. Such analysis and characterizations proving that a free standing hydrophobic/hydrophilic PU/CA Janus fibrous membrane with no solvent residues was successfully prepared.

To verify the wettability of the composited two layers of the Janus membrane, water contact angles (WCA) are tested. Figure 4b,c exhibits the water contact angles of the PU and CA fibrous membranes. A water droplet about 3 µL is allowed to contact the surface of all samples. Accordingly, WCA are 132.5° ± 0.12°, 135.4° ± 0.96°, 136.7° ± 0.40°, and 134.9° ± 0.22° corresponding to PU-6G, PU-8G, PU-10G, and PU-12G, respectively, indicating the PU fibrous layers are hydrophobic (blue line and inserted photos with dotted frames in Figure 4b). For the CA fibrous layers, the WCA are 83.7° ± 0.12°, 88.7° ± 0.64°, 89.1° ± 0.47°, and 89.5° ± 0.06° corresponding to CA-6G, CA-8G, CA-10G, and CA-12G which show hydrophilicity for all CA fibrous layers. The polymers natural property and porous membranes with high surface roughness are the main reasons for their hydrophobicity and hydrophilicity. It also can be seen that the different fiber diameters show weak influence on the wettability. Since there is only slight water contact angle changes when the type of electrospun needles nozzles is over 8G for both PU and CA electrospun fibrous membrane, the electrospun needle nozzle type of 8G is chosen in this work.

Apart from wettability, in order to detect the interaction between water and the hydrophobic, hydrophilic, as well as the Janus fibrous membranes which play important roles in water vapor transmission, the drawing force of the fibrous membranes toward the water droplet was measured by using a micro-force balance system. According to Figure 4d, two testing types, schematically showing as Type 1 and Type 2, were employed. For type 1, a water droplet (5 µL) was brought to contact the membrane and then pulled off according to which the force between the water droplet and the fibrous membranes was probed. Conversely, for Type 2, the water droplet was brought to contact the membrane without pulling off, and the real-time force change was recorded. Meanwhile, according to Type 2, water spreading or adsorbing time by fibrous membrane can be measured.

When measured by Type 1 (Figure 4e), the water droplet contacted the surface and then moved downward, the force gradually increased with increasing the "moving downward" distance (D). Once the water droplet separated from the membrane, the force reached a maximum value (F) after

which it then decreased abruptly. The recorded corresponding force for the fibrous membranes hydrophobic PU-8G, hydrophilic CA-8G and Janus membrane (testing from hydrophobic PU-8G side) was 479.18 μN (D = 1.187 mm), 336.18 μN (D = 1.941 mm) and 569.38 μN (D = 0.046), respectively. Making a comparation between PU-8G and CA-8G, the hydrophobic PU-8G shows higher adhesive force to water at a smaller D value, exhibiting a larger adhesive capacity to water droplet. For the Janus fibrous membrane, the adhesive force reaches to the maximum value at a very smaller D value, indicating that in addition to the hydrophobic force provided by PU-8G layer, water transport from the top PU-8G layer to the bottom CA-8G layer plays an important role in the rapid increase of adhesive force in short time.
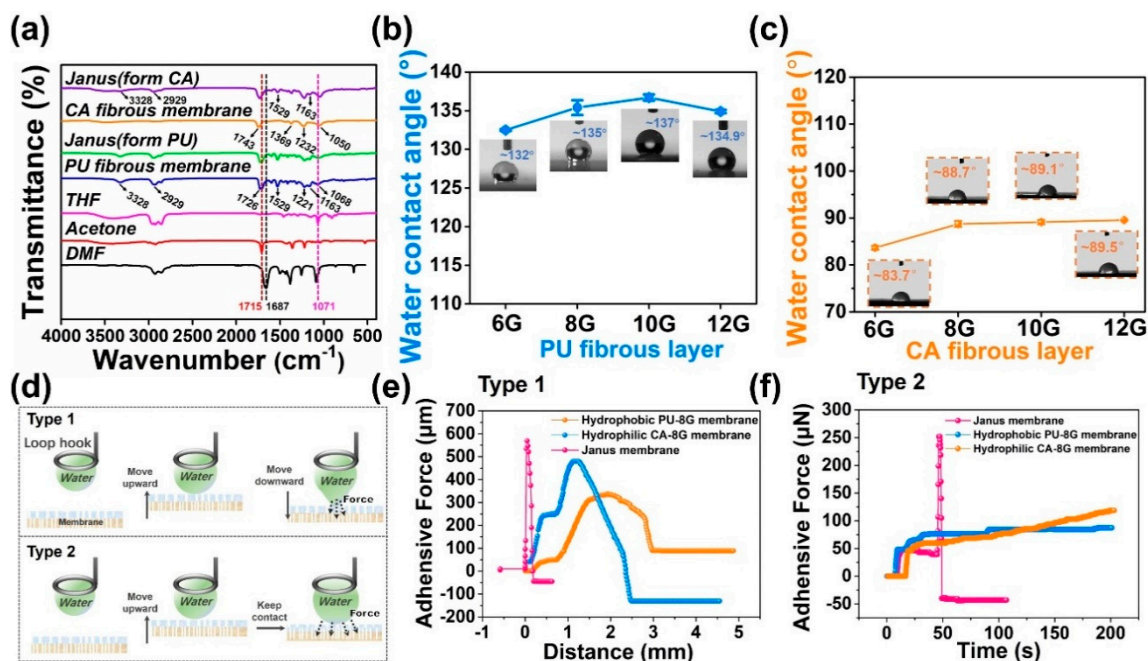

Figure 4. (**a**) Fourier transform infrared spectrometry (FTIR) spectrum of the PU, CA, Janus fibrous membranes, the solvent DMF, THF, acetone. (**b**) Water contact angles of PU-6G, PU-8G, PU-10G, and PU-12G. (**c**) Water contact angles of CA-6G, CA-8G, CA-10G, and CA-12G. (**d**) Schematic diagrams of the two testing types of the force between tiny water droplet and the surface of the membrane. (**e**) Testing type 1: Water droplet (5 μL) was brought to contact the membrane and then pulled off. It enabled to probe the interaction between water droplet and membrane. (**f**) Testing type 2: Water droplet (5 μL) was brought to contact the membrane without pulling off. The real-time force change was recorded.

Figure 4f shows the testing results based on Type 2. Shorter time to reach a peak force suggests faster wicking or spreading of water into the fibrous membrane. It is necessary to point out that for the fibrous surface with water adsorption capacity, once the water droplet makes contact with the surface, it can be adsorbed or spread gradually. The maximum force value appears when the water droplet contacted on the membrane and drops rapidly in a short time, regarded as a shorter time to reach the peak suggesting water spreading or adsorbing. On the contrary, for hydrophobic surface, there is only weak water absorption capacity caused by hydrophobic capillary force, the typical time–force curve has rarely risen or fallen. The recorded time for Janus membrane was 47.16 s, and the time–force curve falls abruptly which indicates the stronger and faster affinity to water. For the hydrophobic PU-8G fibrous membrane, there is no obvious change because of non-adsorption feature of hydrophobic membrane. Once water droplet contacted on the hydrophobic surface, it stays on the surface instead of spreading or getting absorbed. The slight change in force with the increased testing time was caused by the capillary absorption of the hydrophobic surface which keeps the water droplet in Wenzel state or

the water evaporation. Compared to the hydrophobic PU-8G, the hydrophilic CA-8G exhibits obvious change in the time–force curve, which results from the water droplet adsorption and spreading that caused a pull straight downward.

The water vapor transmission capability of the Janus membrane was not only affected by the internal porous structure of the membrane, but also by the wettability on both sides of the membrane. The wettability in this work was mainly governed by the surface roughness. Surface roughness enhances the surface wettability, that is surface roughness makes hydrophobic surface more hydrophobic and hydrophilic surface more hydrophilic. Therefore, in order to explain the influence of surface roughness on wettability, water contact angles of PU and CA membranes prepared by spin-coating (relative smooth surface) and electrospinning (rough surface) were measured respectively (Figure 5). It can be seen that the wettability improves to some extent, such as PU membrane becomes more hydrophobic and CA membrane becomes more hydrophilic.
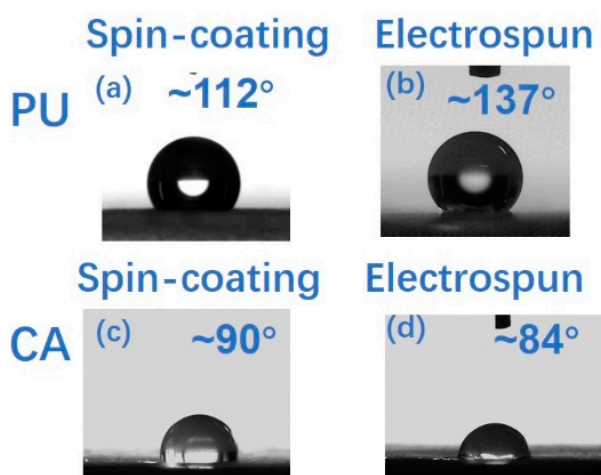

Figure 5. Water contact angles of PU and CA. (**a**) PU membrane prepared by spin-coating; (**b**) electrospun PU membrane; (**c**) CA membrane prepared by spin-coating; (**d**) electrospun CA membrane.

3.3. Enhanced Directional Water Vapor Transmission Capability

To explore the water vapor transmission capability of PU-8G/CA-8G Janus fibrous membranes, the directional water vapor transmission performance was characterized and investigated quantitatively by moisture-management tester (MMT). Figure 6a shows the schematic illustration of the water vapor transmission from the hydrophobic PU-8G side to the hydrophilic CA-8G side, as well as from the reverse direction, that is, from the hydrophilic CA-8G side to hydrophobic PU-8G side. In addition, based on our previous research works, we found that once the thickness of the hydrophobic layer was fixed, the directional water transport ability is highly dependent on the thickness of the hydrophilic layer [18,20,21]. Herein, the thickness of hydrophobic PU layer was fixed, and the thickness of the hydrophilic CA layer was changed by adjusting its electrospinning time. Figure 6b presents the water content on both the top and bottom surface of the Janus membranes where water was dropped on the hydrophobic PU and hydrophilic CA side, respectively. It is interesting to note that (i) the water content when water drops from the hydrophobic PU-8G to hydrophilic CA-8G was higher than that in the reverse direction for all as-prepared membranes; (ii) when the CA electrospinning time is short (not more than 5 min), the water content of the hydrophobic PU-8G was higher than that of the hydrophilic CA-8G. However, when the CA electrospinning time was lengthened (more than 10 min), the water content of the hydrophilic CA-8G was higher than that of the hydrophobic PU-8G, inversely. The reason for this phenomenon was that when the CA electrospinning time is short, the capillary force generated by the CA layer was small, so when the water drops on the hydrophobic PU-8G, a large amount of water remains on the surface. When water drops from the hydrophilic CA-8G, the water quickly penetrates the CA layer and reaches the PU layer, so the water content on the PU-8G side was higher. As the CA electrospinning

time was lengthened, the thickness of the CA layer was increased and the hydrophilic ability was increased, so when water was dropped from the PU-8G, the water content of the PU layer was lowered. However, when water was dropped from the CA-8G, the CA layer's ability to absorb and spread the water increases during the specified test time (120 s) because of the increase in the thickness of the CA layer until the criticality is reached. Therefore, the water content on the CA-8G was higher. iii) When the CA-8G electrospinning time reached 15 min, the water content transport from hydrophobic PU-8G side to hydrophilic CA-8G side reached a minimum value of ((1203.7 ± 17.8)%). This phenomenon was consistent with the one-way transport capacity results, indicating that the combination of PU layer and CA layer reaches the best state and the wicking effect of Janus membrane was the best. Subsequently, the one-way water transport of the Janus membranes from both the hydrophobic to hydrophilic side and from hydrophilic to hydrophobic side were measured. It is obvious that the one-way transport capacity from hydrophobic PU side to hydrophilic CA side of all as-prepared Janus membranes with different CA-8G electrospinning time were higher than those from the reverse direction. When the electrospinning time of CA-8G was 15 min, the one-way transport capacity reached to the maximum value. They were about 296.7% and −145.5% from the hydrophobic PU-8G side and from the hydrophilic CA-8G, respectively. Meanwhile, they were still higher than the individual PU (−25.9%, electrospun 5 min) and CA (49.8%, electrospun 15 min) layers.
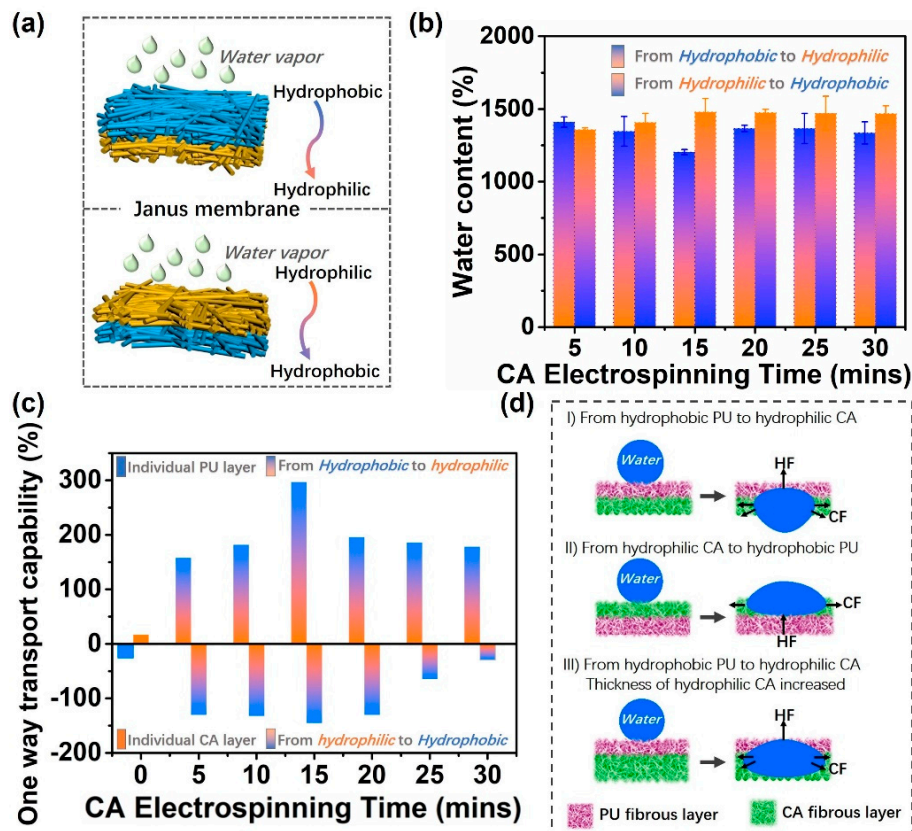

Figure 6. (**a**) Schematic illustration of water vapor transmission. (**b**) Moisture-management testing (MMT) results of hydrophobic PU/hydrophilic CA Janus fibrous membrane with different hydrophilic CA-8G electrospinning times. The water contents tested from the hydrophobic side to hydrophilic side and the reverse direction were taken into consideration. (**c**) The measurements of the one way transport capacity of all as-prepared Janus fibrous membranes. (**d**) The mechanism of the enhanced water vapor transmission.

The enhanced amount of water vapor transmission from the hydrophobic PU side to the hydrophilic CA side than that in reverse direction can be attributed to the asymmetric wettability of the Janus

membrane itself. The mechanism is illustrated in Figure 6d. When water vapor is attached to the hydrophobic PU-8G layer, the droplets exhibited a spherical or a hemispherical shape ((I) in Figure 6d), as water exists in Wenzel state or Wenzel-Cassie state and is subjected to the hydrophobic force (HP) because of the hydrophobicity of the surface. The tiny droplets grew larger with increasing time. When the gravity of water droplet overcomes the HP, it attached to the hydrophilic CA-8G layer, and the hydrophilic capillary force (CF) caused tiny water droplets to get absorbed and spread in the hydrophilic layer. Meanwhile, fresh hydrophobic surfaces were provided to capture more water droplets. Once the thickness of hydrophilic CA-8G increased ((II) in Figure 6d), the mass of the fibrous membrane increased and the pores between the fibers decreased, making it more difficult for the water vapor to pass through. In addition, it's necessary to mention that when the hydrophilic CA was electrospun in a very short time, the CA layer was thin. It can be understood that the hydrophilic micro/nanopores form abundant capillaries can rapidly absorb water and allow the directional transmission. If the hydrophilic CA layer was very thin, there was no enough CF to "drag" tiny water droplet from the hydrophobic PU layer efficiently and thus cannot guarantee the best one-way transport capability. Therefore, both the water vapor transmission and one-way transmission capacity decreased. Compared to (I) in Figure 6d, once tiny water droplet attached on the hydrophilic CA-8G layer ((III) in Figure 6d), they spread or were adsorbed much more quickly resulting from the CF, and the HF prevented its further penetration or absorption, which led to less amount of water vapor transmission at the same measure time.

The one-way transmission capacity (%) of this work has reached the GB-4 standard in GB/T 21655.2-2009 (Textiles-Evaluation of absorption and quick-drying—Part:2 Method for moisture management tests), which is very closed to the GB-5 standard. The GB/T 21655.2-2009 standard is a Chinese national standard, divided into five standards in a scale of 1–5. When the one-way transport capacity value is between 200 and 300, it corresponds to the level 4 standard. While when the one-way transport capacity value is >300, it reaches the level 5 standard. And the greater the standard number, the better the one-way transport capacity of the membrane. In addition, we have also conducted research on related work in recent years and found that other works have also achieved excellent results. The details of the investigation show that there is a slight difference between our work and the works previously reported. The structure and properties of the material are the main factors contributing to the difference in the results. Moreover, there are variable testing methods and evaluation standards in reported works showed in Table 1. Qualitatively, the hydrophobic/hydrophilic Janus fibrous membranes, as well as the membranes which have been reported in previous works, perform well in the case of their testing standards.

Table 1. Investigation of the one-way transport capability of previously reported works and this work.

One-Way Transport Capability (%)	Testing Time (s)	Reference
861	120	[40]
1413	500	[41]
1021	500	[42]
1245	500	[43]
297	120	This work

4. Conclusions

In summary, the hydrophobic/hydrophilic Janus fibrous membranes were successfully fabricated by electrospinning. Taking advantages of the asymmetric wettability of the Janus membrane, water vapor transmission capacity is enhanced when tiny water droplets pass from the hydrophobic side to the hydrophilic side than that from the reverse direction. Such work uncovers the asymmetric wettability-related-property of fibrous membrane, and exhibits great potential in efficient moisture permeable fabric design and fabrication which provide a cooler and drier micro climate to satisfy the personal comfort, and for designing high efficiency water or fog harvesters.

References

1. Wu, J.; Zhou, H.; Wang, H.X.; Shao, H.; Yan, G.L.; Lin, T. Novel Water Harvesting Fibrous Membranes with Directional Water Transport Capability. *Adv. Mater. Interfaces* **2019**, *6*, 1801529. [CrossRef]
2. Zhang, S.; Huang, J.; Chen, Z.; Lai, Y. Bioinspired Special Wettability Surfaces: From Fundamental Research to Water Harvesting Applications. *Small* **2017**, *13*, 1602992. [CrossRef] [PubMed]
3. Bai, H.; Sun, R.; Ju, J.; Yao, X.; Zheng, Y.; Jiang, L. Large-Scale Fabrication of Bioinspired Fibers for Directional Water Collection. *Small* **2011**, *7*, 3429–3433. [CrossRef] [PubMed]
4. Cao, M.; Xiao, J.; Yu, C.; Li, K.; Jiang, L. Hydrophobic/Hydrophilic Cooperative Janus System for Enhancement of Fog Collection. *Small* **2015**, *11*, 4379–4384. [CrossRef] [PubMed]
5. Zhao, Y.; Wang, H.; Zhou, H.; Lin, T. Directional Fluid Transport in Thin Porous Materials and its Functional Applications. *Small* **2017**, *13*, 1601070. [CrossRef] [PubMed]
6. Dong, Y.; Thomas, N.L.; Lu, X. Electrospun Dual-Layer Mats with Covalently Bonded Zno Nanoparticles for Moisture Wicking and Antibacterial Textiles. *Mater. Des.* **2017**, *134*, 54–63. [CrossRef]
7. Babar, A.A.; Miao, D.Y.; Ali, N.; Zhao, J.; Wang, X.F.; Yu, J.Y.; Ding, B. Breathable and Colorful Cellulose Acetate-Based Nanofibrous Membranes for Directional Moisture Transport. *ACS Appl. Mater. Interfaces* **2018**, *10*, 22866–22875. [CrossRef]
8. Parker, A.R.; Lawrence, C.R. Water capture by a desert beetle. *Nature* **2001**, *414*, 33–34. [CrossRef]
9. Nørgaard, T.; Dacke, M. Fog-basking behaviour and water collection efficiency in Namib Desert Darkling beetles. *Front. Zool.* **2010**, *7*, 1–8. [CrossRef]
10. Gans, C.; Merlin, R.; Blumer, W.F.C. The water-collecting mechanism of Moloch horridus re-examined. *Amphib.-Reptil.* **1982**, *3*, 57–64.
11. Comanns, P.; Effertz, C.; Hischen, F.; Staudt, K.; Böhme, W.; Baumgartner, W. Moisture harvesting and water transport through specialized micro-structures on the integument of lizards. *Beilstein J. Nanotechnol.* **2011**, *2*, 204–214. [CrossRef]
12. Zheng, Y.; Bai, H.; Huang, Z.; Tian, X.; Nie, F.Q.; Zhao, Y.; Zhai, J.; Jiang, L. Directional water collection on wetted spider silk. *Nature* **2010**, *463*, 640–643. [CrossRef]
13. Geng, H.; Bai, H.; Fan, Y.; Wang, S.; Ba, T.; Yu, C.; Cao, M.; Jiang, L. Unidirectional water delivery on a superhydrophilic surface two-dimensional asymmetrical wettability barriers. *Mater. Horiz.* **2018**, *5*, 303–308. [CrossRef]
14. Pang, C.; Kim, S.M.; Rahmawan, Y.; Suh, K.-Y. Beetle-inspired bidirectional, asymmetric interlocking using geometry-tunable nanohairs. *ACS Appl. Mater. Interfaces* **2012**, *4*, 4225–4230. [CrossRef]
15. Wu, J.; Zhang, L.; Wang, Y.; Wang, P. Efficient and Anisotropic Fog Harvesting on a hybrid and directional surface. *Adv. Mater. Interfaces* **2017**, *4*, 1600801. [CrossRef]
16. Chen, Y.; Wang, L.; Xue, Y.; Jiang, L.; Zheng, Y. Bioinspired tilt-angle Fabricated structure gradient fibers: Micro-drops fast transport in a long-distance. *Sci. Rep.* **2013**, *3*, 2927–2934. [CrossRef]
17. Xue, Y.; Chen, Y.; Wang, T.; Jiang, L.; Zheng, Y. Directional Size-Triggered Microdroplet Target Transport on Gradient-Step Fibers. *J. Mater. Chem. A* **2014**, *2*, 7156–7160. [CrossRef]
18. Wang, H.; Ding, J.; Dai, L.; Wang, X.; Lin, T. Directional water-transfer through fabrics induced by asymmetric wettability. *J. Mater. Chem.* **2010**, *20*, 7938–7940. [CrossRef]
19. Zhou, H.; Wang, H.; Niu, H.; Lin, T. Superphobicity/philicity Janus Fabrics with Switchable, Spontaneous, Directional Transport Ability to Water and Oil Fluids. *Sci. Rep.* **2013**, *3*, 2964–2968. [CrossRef]

20. Wu, J.; Wang, N.; Wang, L.; Dong, H.; Zhao, Y.; Jiang, L. Unidirectional water-penetration composite fibrous film via electrospinning. *Soft Matter* **2012**, *8*, 5996–5999. [CrossRef]

21. Tian, X.; Li, J.; Wang, X. Anisotropic liquid penetration arising from a cross-sectional wettability gradient. *Soft Matter* **2012**, *8*, 2633–2637. [CrossRef]

22. Cao, M.; Li, K.; Dong, Z.; Yu, C.; Yang, S.; Song, C.; Liu, K.; Jiang, L. Superhydrophobic "Pump": Continuous and spontaneous antigravity water delivery. *Adv. Funct. Mater.* **2015**, *25*, 4114–4119. [CrossRef]

23. Nazir, A.; Hussain, T.; Abbas, G.; Ahmed, A. Effect of design and method of creating wicking channels on moisture management and air permeability of cotton fabrics. *J. Nat. Fibers* **2015**, *12*, 232–242. [CrossRef]

24. Yang, H.-C.; Hou, J.; Chen, V.; Xu, Z.-K. Janus Membranes: Exploring Duality for Advanced Separation. *Angew. Chem. Int. Ed.* **2016**, *55*, 13398–13407. [CrossRef]

25. Zuo, G.; Wang, R. Novel membrane surface modification to enhance anti-oil fouling property for membrane distillation application. *J. Membr. Sci.* **2013**, *447*, 26–35. [CrossRef]

26. Zhou, H.; Guo, Z. Superwetting Janus membranes: Focusing on unidirectional transport behaviors and multiple applications. *J. Mater. Chem. A* **2019**, *7*, 12921–12950. [CrossRef]

27. Chew, N.G.P.; Zhao, S.; Malde, C.; Wang, R. Polyvinylidene fluoride membrane modification via oxidant-induced dopamine polymerization for sustainable direct-contact membrane distillation. *J. Membr. Sci.* **2018**, *563*, 31–42. [CrossRef]

28. Yang, H.-C.; Xie, Y.; Hou, J.; Cheetham, A.K.; Chen, V.; Darling, S.B. Janus Membranes: Creating Asymmetry for Energy Efficiency. *Adv. Mater.* **2018**, *30*, 1801495. [CrossRef]

29. Chew, N.G.P.; Zhang, Y.; Goh, K.; Ho, J.S.; Xu, R.; Wang, R. Hierarchically Structured Janus Membrane Surfaces for Enhanced Membrane Distillation Performance. *ACS Appl. Mater. Interfaces* **2019**, *11*, 25524–25534. [CrossRef]

30. Bai, H.; Ju, J.; Zheng, Y.; Jiang, L. Functional fibers: Functional Fibers with Unique Wettability Inspired by Spider Silks. *Adv. Mater.* **2012**, *24*, 2786–2791. [CrossRef]

31. Wu, J.; Wang, N.; Zhao, Y.; Wang, L.; Dong, H.; Zhao, Y.; Jiang, L. Electrospun porous structure fibrous film with high oil adsorption capacity. *ACS Appl. Mater. Interfaces* **2012**, *4*, 3207–3212. [CrossRef]

32. Mokhtar, N.M.; Lau, W.J.; Ismail, A.F.; Ng, B.C. Physicochemical study of polyvinylidene fluoride-Cloisite15A composite membranes for membrane distillation application. *RSC Adv.* **2014**, *4*, 63367–63379. [CrossRef]

33. Tsilomelekis, G.; Josephson, T.R.; Nikolakis, V.; Caratzoulas, S. Origin of 5-Hydroxymethylfurfural Stability in Water/Dimethyl Sulfoxide Mixtures. *ChemSusChem* **2014**, *7*, 117–126. [CrossRef]

34. Sabrina, A.; Fabiano, B.S.; Arnaldo, F.S.; Ieda, S.S.; Roy, E.B. Infrared spectral evidence and DFT calculations of hydrogen-bonding and molecular structures of acetogenins. *J. Mol. Struct.* **2017**, *1130*, 174–180.

35. Jadhav, D.L.; Karthick, N.K.; Kannan, P.P.; Shanmugam, R.; Elangovan, A.; Arivazhagan, G. Molecular interaction forces in acetone + ethanol binary liquid solutions: FTIR and theoretical studies. *J. Mol. Struct.* **2017**, *1130*, 497–502. [CrossRef]

36. Son, W.K.; Youk, J.H.; Lee, T.S.; Park, W.H. Electrospinning of ultrafine cellulose acetate fibers: Studies of a new solvent system and deacetylation of ultrafine cellulose acetate fibers. *J. Polym. Sci. Polym. Phys.* **2004**, *42*, 5–11. [CrossRef]

37. Ertas, Y.; Uyar, T. Fabrication of cellulose acetate/polybenzoxazine cross-linked electrospun nanofibrous membrane for water treatment. *Carbohyd. Polym.* **2017**, *177*, 378–387. [CrossRef]

38. Guo, Z.; Tang, G.; Zhou, Y.; Liu, S.; Hou, H.; Chen, Z.; Chen, J.; Hu, C.; Wang, F.; Smedt, S.C.D.; et al. Fabrication of Sustained-release CA-PU Coaxial Electrospun Fiber Membranes for Plant Grafting Application. *Carbohydr. Polym.* **2017**, *169*, 198–205. [CrossRef]

39. Gabriel, L.P.; Rodrigues, A.A.; Macedo, M.; Jardini, A.L.; Filho, R.M. Electrospun polyurethane membranes for Tissue Engineering applications. *Mater. Sci. Eng. C Mater.* **2017**, *72*, 113–117. [CrossRef]

40. Zeng, C.; Wang, H.; Zhou, H.; Lin, T. Directional Water Transport Fabrics with Durable Ultra-High One-Way Transport Capacity. *Adv. Mater. Interfaces* **2016**, *3*, 1600036. [CrossRef]

41. Babar, A.A.; Wang, X.; Iqbal, N.; Yu, J.; Ding, B. Tailoring Differential Moisture Transfer Performance of Nonwoven/Polyacrylonitrile-SiO$_2$ Nanofiber Composite Membranes. *Adv. Mater. Interfaces* **2017**, *4*, 1700062. [CrossRef]

42. Miao, D.; Huang, Z.; Wang, X.; Yu, J.; Ding, B. Continuous, Spontaneous, and Directional Water Transport in the Trilayered Fibrous Membranes for Functional Moisture Wicking Textiles. *Small* **2018**, *14*, 1801527. [CrossRef]

43. Wang, X.; Huang, Z.; Miao, D.; Zhao, J.; Yu, J.; Ding, B. Biomimetic Fibrous Murray Membranes with Ultrafast Water Transport and Evaporation for Smart Moisture-Wicking Fabrics. *ACS Nano* **2019**, *13*, 1060–1070. [CrossRef]